Frontiers of Information Technology & Electronic Engineering
www.jzus.zju.edu.cn; engineering.cae.cn; www.springerlink.com
ISSN 2095-9184 (print); ISSN 2095-9230 (online)
E-mail: jzus@zju.edu.cn

Novel design of a compact tunable dual band wireless power transfer (TDB-WPT) system for multiple WPT applications#

Hany A. ATALLAH[1], Rasha Hussein AHMED‡[1], Adel B. ABDEL-RAHMAN[2]

[1]*Department of Communications and Electronics, Faculty of Engineering, South Valley University, Qena 83523, Egypt*

[2]*Egypt-Japan University of Science and Technology, Alexandria 21934, Egypt*

E-mail: hany.mohamed@ejust.edu.eg; rasha.h.ahmed@eng.svu.edu.eg; adel.bedair@ejust.edu.eg

Received Dec. 26, 2022; Revision accepted Aug. 6, 2023; Crosschecked Mar. 11, 2024

Abstract: In this study we present the design and realization of a tunable dual band wireless power transfer (TDB-WPT) coupled resonator system. The frequency response of the tunable band can be controlled using a surface-mounted varactor. The transmitter (Tx) and the receiver (Rx) circuits are symmetric. The top layer contains a feed line with an impedance of 50 Ω. Two identical half rings defected ground structures (HR-DGSs) are loaded on the bottom using a varactor diode. We propose a solution for restricted WPT systems working at a single band application according to the operating frequency. The effects of geometry, orientation, relative distance, and misalignments on the coupling coefficients were studied. To validate the simulation results, the proposed TDB-WPT system was fabricated and tested. The system occupied a space of 40 mm×40 mm. It can deliver power to the receiver with an average coupling efficiency of 98% at the tuned band from 817 to 1018 MHz and an efficiency of 95% at a fixed band of 1.6 GHz at a significant transmission distance of 22 mm. The results of the measurements accorded well with those of an equivalent model and the simulation.

Key words: Defected ground structure (DGS); Surface-mounted; Tunable dual band wireless power transfer (TDB-WPT); Varactor

https://doi.org/10.1631/FITEE.2200664 **CLC number:** TM724

1 Introduction

The wireless power transfer (WPT) technique is a means for delivering electric power from a source to an end device without physical wires or contacts. Current research on WPT is driven mainly by the increasing requirements of wire-free portable electronic devices (Garnica et al., 2013; Hekal et al., 2017). WPT is a promising technology for easy and free power transmission, which will facilitate the charging of many portable electronic devices used in our daily life. Almost all studies consider how to restrict the use of wires or cables within a narrow range. Jolani et al. (2014) suggested printed spiral coils for a planar magnetically coupled resonant WPT system. However, the system achieved an efficiency of only 81.68% at a transmission distance of 10 cm with a size of 100 mm×100 mm. Wireless sensors were introduced by Belo et al. (2017) for article tracking, location detection, temperature sensors, and many other systems. Their system was operated at 1.6 GHz for power and at 2.3 GHz for data transfer. Minnaert and Stevens (2018) used a mixed topology in WPT using inductive coupling for transferring power and capacitive coupling for maximizing the power transfer. Dual band wireless power transfer (DB-WPT) using dual mode inductors was introduced by Barakat et al. (2019). The system achieved efficiencies of 70% at 90.3 MHz and 69% at 138.8 MHz,

‡ Corresponding author

Electronic supplementary materials: The online version of this article (https://doi.org/10.1631/FITEE.2200664) contains supplementary materials, which are available to authorized users

ORCID: Hany A. ATALLAH, https://orcid.org/0000-0001-5541-2326; Rasha Hussein AHMED, https://orcid.org/0000-0003-0753-1907

with a transmission distance of 40 mm and a size of 50 mm×50 mm. WPT technique is applied in many applications (Wang et al., 2005; Yang et al., 2017). In biomedical applications, the WPT system consists of four coils for deep brain simulation (Belo et al., 2017). Wireless power has been introduced to many fields, such as the control of robots and drones. A remotely controlled mobile robot described by Sun et al. (2018) can perform a number of jobs, move to specific positions, and complete jobs. The performance of remote control and monitoring applications over commercial wireless communication networks was enhanced by Liu Y and Jäntti (2006). Huh et al. (2011) and Xu et al. (2019) used a WPT technique for recharging electrical vehicles. Longitudinally misalignment-insensitive DB-WPT and data transfer systems have been used for detecting the positions of fast-moving vehicles (Lee et al., 2019). A new E-shaped patterned ground structure was proposed by modifying the most recently developed T-shaped resonator and adopting the U-slot resonator geometry (Huang and Lee, 2009). An optimal design of wireless power transmission links for mm-sized biomedical implants was proposed by Ahn and Ghovanloo (2016). Exploitation of a dual-band cell phone antenna for near-field WPT was presented by del Prete et al. (2015), and defected ground structure (DGS) techniques used for compact near-field WPT systems were presented by Dautov et al. (2020). Jeshma and George (2020) studied an magnetoresistance (MR) sensor based coil alignment sensing system for wirelessly charged electric vehicles (EVs). Verma et al. (2021) measured and characterized a newly developed novel miniature wireless information and power transfer (WIPT) system. A compact multi-frequency system design for simultaneous wireless information and power transfer (SWIPT) applications was studied by Dautov et al. (2021). A DB-WPT system proposed by Atallah et al. (2020) was designed using a C-shaped resonator at the top and a spiral DGS at the ground. The design operated at 0.260 GHz with an efficiency of 91.2% and at 0.490 GHz with an efficiency of 79.4%. A capacitively loaded C-shaped DGS resonator used for a DB-WPT system with resonance frequencies of 0.3 and 0.9 GHz was studied by Atallah et al. (2019) and achieved efficiencies of 99% and 91%, respectively. The system had a size of 20 mm×20 mm and was targeted to transfer power at a transmission distance of 10 mm. Bow tie DGS resonators were used by Saad et al. (2018) to enhance the figure of merit (FoM) in a DB-WPT system. The system achieved FoMs of 0.78 at 470 MHz and 0.96 at 730 MHz. Tahar et al. (2017) developed a structure in which the circular DGS resonators were coupled back to back to transfer power. The dimension was 30 mm×15 mm and it operated with an efficiency of 71% at both 0.3 and 0.7 GHz resonance frequencies. A dual-band reconfigurable WPT system comprising a dual-band transmitter (Tx) and multiple dual band receivers (Rxs) was proposed by Liu M and Chen (2019). WPT systems with efficiency tracking circuits for dynamic environments were described by Kung et al. (2019). An overlapping DGS was used by Tahar et al. (2018) to reduce the size of the dual band system by 50%. With a dimension of 15 mm×15 mm, the manufactured system achieved efficiencies of 71% at 0.45 GHz and 73% at 0.95 GHz. Sharaf et al. (2019) suggested transferring wireless power at two resonance frequencies by using the electromagnetic (EM) resonant coupling between the Tx and the Rx. The system operated with efficiencies of 80% at 300 MHz and 73% at 675 MHz. They studied four different DGS shapes: triangular, rectangular, square, and circular. The system achieved an efficiency of 80% with a transmission distance of 17 mm. Variable inductance was introduced by Fereshtian and Ghalibafan (2020) for enhancing the impedance matching and efficiency of DB-WPT.

In this study we introduce a novel and compact design to transfer wireless power in dual bands with a reconfiguration operation at one band for near-field applications. The reconfiguration of the proposed design is achieved by using a single varactor diode. In contrast, most previous systems designed for WPT have fixed bands according to the designed resonance frequency without any flexibility for changing the working frequency.

Previous studies by Saad et al. (2018), Atallah et al. (2019), and Sharaf et al. (2019) discussed DB-WPT systems. These systems can operate at dual bands by incorporating fixed tin welded surface-mounted capacitors inside the designs, which results in fixed bands of operation. For achieving the tunability operation, the designs should have a reconfigurable element that changes the frequency of operation without changing the DGS geometry, but this requires more investigation. The new geometry composed of a ring shape

was chosen due to its advantages such as in changing the frequency, transfer range, or orientation.

The proposed system operates in dual bands: the first is tuned from 817 to 1018 MHz and the second is fixed at 1.6 GHz. Some applications such as space-based sensors are operated at 1.6 GHz (Belo et al., 2017), while the low frequency around 1000 MHz can be used for biomedical applications (Hu and Georgakopoulos, 2015).

The proposed system can be used for multifunction applications such as transferring power for biomedical applications and wireless sensors. Further, the tuned band can be used for transferring power and the fixed band for transferring data. An integrated wireless power supply system for a pacemaker requires a supply that maintains the heartbeat rhythm and transfers power back to track the heart's performance. Therefore, the WPT system needs multiple bands to be used in such applications: at least one for WPT and one for data transmission. These requirements pushed researchers to design WPT systems at low-frequency bands for power transfer and at high-frequency bands for data transmission by using a dual band system. Yang et al. (2017) reported a device for such an application.

To address the restriction of previous systems which were designed for a specific application according to the working resonance frequency, this new system is designed to be tunable and suitable for multiple WPT applications with different resonance frequencies. The tunable band added to the new WPT system allows the system to be used for multifunction or multiple applications.

2 DBSF analysis

Originally, the dual band stop filter (DBSF) was produced on Rogers 5880 laminate having a relative permittivity of ε_r=2.2, a substrate thickness of h_{sub}= 0.508 mm, and a metal thickness of t=35 μm. The top layer consists of a feed line having an impedance of 50 Ω. The bottom layer consists of two half rings loaded by a varactor (SMV1405) at one side of the ring for miniaturization and reconfiguration operations (Fig. 1). The detailed simulation parameters for the proposed DBSF shown in Fig. 1 are listed in Table 1.

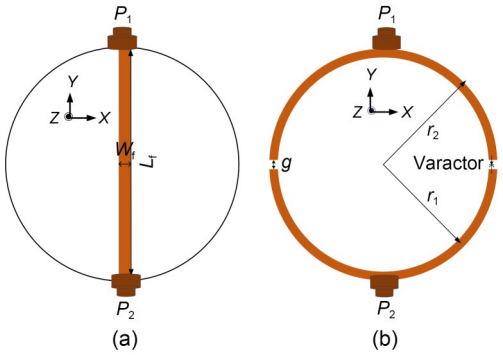

Fig. 1 Dual band stop filter: (a) top view; (b) bottom view (P_1: port 1; P_2: port 2)

Table 1 Component parameters of the dual band stop filter

Parameter	Value/Type
Substrate	Rogers 5880
ε_r	2.2
h_{sub} (mm)	0.508
r_1 (mm)	18
r_2 (mm)	20
g (mm)	1
W_f (mm)	1.57
L_f (mm)	40
C (pF)	10
Varactor	SMV1405
L_1 (nH)	47

L_f: length of a feedline; W_f: width of a feedline; C: capacitor; r_1: small half ring; r_2: large half ring; g: gap between the two rings; L_1: surface mounted inductor which is mounted in structure to isolate the direct current from the alternative current

Fig. 2 illustrates the LC equivalent circuit of the DBSF. L_{P1} and C_{P1} are the inductance and capacitance at the first resonance frequency, respectively. L_{P3} and C_{P3} are the inductance and capacitance at the second resonance frequency, respectively.

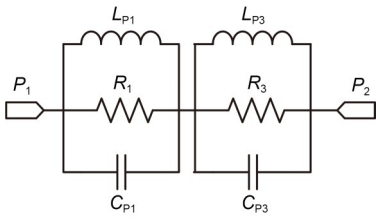

Fig. 2 Equivalent circuit of the proposed dual band stop filter

The values of capacitors and inductors in the LC circuit model are calculated using Eqs. (1) and (2), respectively (Abdel-Rahman et al., 2004):

$$C_{\mathrm{P}}=\frac{5f_{\mathrm{c}}}{\pi\left(f_{\mathrm{o}}^{2}-f_{\mathrm{c}}^{2}\right)}, \tag{1}$$

$$L_{\mathrm{P}}=\frac{250}{C_{\mathrm{P}}\left(\pi f_{\mathrm{o}}\right)^{2}}, \tag{2}$$

where f_{c} is the cutoff frequency and f_{o} is the pole frequency. At the first resonance f_{c1}=0.885 60 GHz and f_{o1}=0.910 78 GHz, the capacitor C_{P1}=31.1 pF and L_{P1}=0.9787 nH. At the second resonance f_{c2}=1.515 50 GHz and f_{o2}=1.589 30 GHz, the capacitor C_{P3}=10.52 pF and L_{P3}=0.9526 nH. Fig. 3 shows a comparison between the simulation results using computer simulation technology (CST) and the equivalent circuit by advanced design system (ADS).

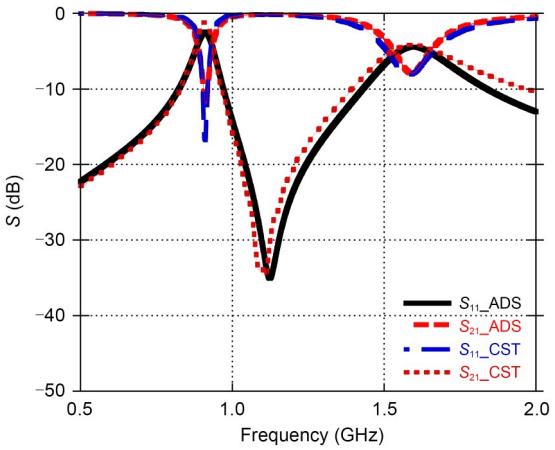

Fig. 3 Comparison between the dual band stop filter in computer simulation technology (CST) and advanced design system (ADS) programs

The magnetic field distributions of the proposed design are shown in Fig. 4. Fig. 4a shows the regularity of the field distributions at the two HR-DGSs for the filter without the loading varactor at the resonance at 1.5 GHz. Figs. 4b and 4c show the magnetic field distributions for the filter with the loading varactor (SMV1405). Fig. 4b shows that the HR-DGS with the varactor acts as a band stop filter (BSF) and absorbs the resonance frequency at 1.5 GHz. Fig. 4c shows the HR-DGS with the varactor acts as a BSF and absorbs a resonance frequency at 817 MHz. The TDB-WPT system contains a two-resonance circuit due to the two HR-DGSs in the ground. The resonance frequency is calculated according to the length of the structure. The two HR-DGSs have the same

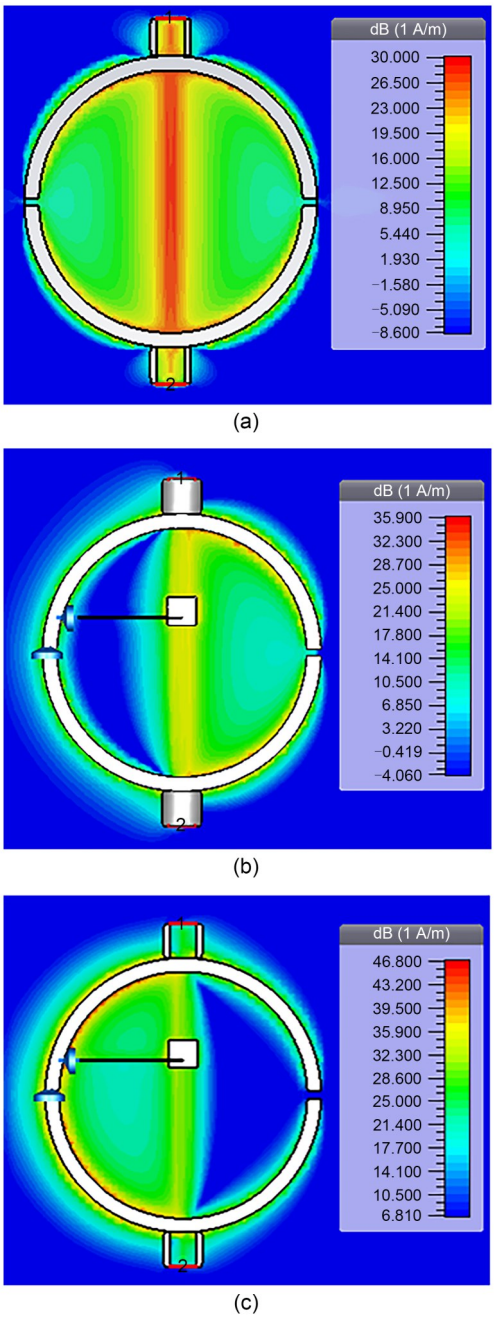

Fig. 4 Magnetic field distributions over the proposed design: (a) without a varactor at 1.5 GHz; (b) with a varactor at a fixed band of 1.5 GHz; (c) with a varactor at the tuned band of 817 MHz

length and width, which leads to the same resonance frequency of 1.6 GHz, as shown in equation $F=\frac{c}{l\sqrt{\varepsilon_{\mathrm{eff}}}}=\frac{3\times10^{8}\ \mathrm{m/s}}{2\pi\times20\times10^{-3}\ \mathrm{m}\times\sqrt{1.87}}$=1.7 GHz, where c is the velocity, l is the circumference of a circle, and $\varepsilon_{\mathrm{eff}}$ is the effective dielectric constant.

A single varactor is added to one HR-DGS. That means the capacitance to one of the HR-DGS circuits is increased and the resonance frequency is reduced according to the equation $f_r = \frac{1}{2\pi\sqrt{LC}}$ from 1.6 GHz to a tuned dual band from 817 to 1018 MHz, according to the type of varactor. Details of the resonance frequency can be seen in Section 1 of the supplementary materials.

3 TDB-WPT system

When two DBSFs are coupled back to back, the power is transferred from the Tx circuit to the Rx circuit via the EM coupling. The new ring shape geometry of the structure was chosen due to its advantages such as in changing frequency, transfer range, and orientation. The dimensions of the ring were chosen according to the desired frequency. Formerly, the dielectric material ε_r and its thickness were selected to be suitable for filtering applications, and the type of varactor was chosen according to the required frequency band. Changing the varactor type will produce a change in the capacitance of the whole system. Hence, the first resonance frequency of the TDB-WPT system will be altered without any change at the second resonance frequency, due to the chosen position of the varactor over the resonator. The surface-mounted capacitor connected between the top and bottom layers is selected to adjust the matching of the structure. The structure of the TDB-WPT system is presented in Fig. 5. The top layer contains a feedline with a length of L_f=40 mm and a width of W_f=1.57 mm. The bottom layer contains two HR-DGSs loaded at one side and using a varactor diode SMV1405. The varactor diode is used to achieve the tunability function of the proposed design to be used at multiple frequencies and in several WPT applications. This design has the same dimensions and specifications as the DBSF discussed in Section 2, except that a matching capacitor C is added at the end of the feedline between the top and bottom views for adjusting the matching between the two coupled resonator systems.

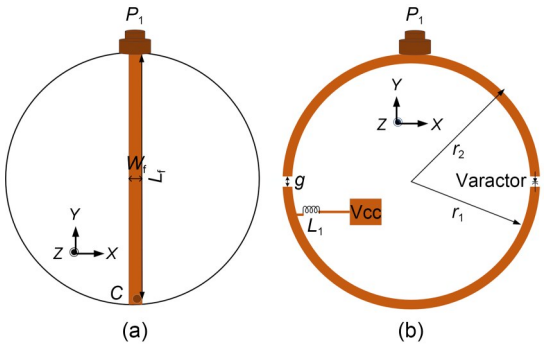

Fig. 5 Top layer (a) and bottom layer (b) of the tunable dual band wireless power transfer system (Vcc: volt current condenser)

Fig. 6a shows the equivalent LC model of the TDB-WPT system. The Tx and Rx circuits are identical. For the first resonance frequency, L_{P1}=L_{P2} and C_{P1}=C_{P2}; for the second resonance frequency, L_{P3}=L_{P4} and C_{P3}=C_{P4}. M_1 is the mutual coupling between the Tx and the Rx in the first resonance. M_2 is the mutual coupling between the Tx and the Rx in the second resonance.

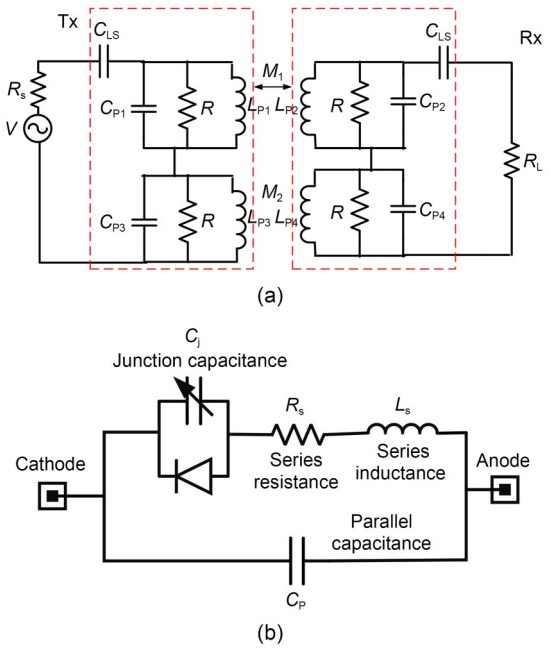

Fig. 6 *LC* equivalent circuit (a) and circuit of the SMV1405 (b)

The equivalent circuit of the varactor diode (SMV1405) is shown in Fig. 6b (Atallah et al., 2016). It consists of a junction capacitance C_j, a series inductance L_s=0.7 nH, a series resistance R_s=0.8 Ω, and a parallel capacitance C_P=0.05 pF. The resonance frequency can be adjusted by tuning the junction capacitance of the attached varactor. When the value of the junction capacitance is changed from low to high,

contrariwise the resonance frequency changes from high to low.

There are several techniques for frequency reconfiguration. Most are realized using physical adjustment, electrical switching, and optical switching. These techniques are used to tune the frequency characteristics of the design. They are flexible for wireless devices by altering their operating frequency to operate at a desired band. To develop an electronically reconfigurable filter, active switching or tuning elements need to be integrated within the filtering structure such as semiconductor p-i-n and varactor diodes, radio frequency microelectromechanical systems (RF-MEMSs), or high-performance complementary metal oxide semiconductors (CMOSs). The varactor diode is the most suitable electrical type for compact printed circuits due to its low cost, easy realization, and availability in commercial markets. The type of varactor is chosen according to the required frequency band. The resonance frequency can be calculated using $f_r=\frac{1}{2\pi\sqrt{LC}}$, and the inductance and the capacitance are used to control the resonance frequency. The inductance can be changed by changing the geometry and the size of the structure. The capacitance can be adjusted by using the new capacitor or the single varactor. The varactor is used to provide a large range of capacitance by changing the amount of direct current (DC) voltage that is applied to the cathode according to the data sheet of the varactor diode. That means more than one resonance frequency (multiple applications) can be obtained with only a single electric element in the circuit. To change the resonance frequency of the previous WPT system, the geometry of the structure is changed or the capacitor in the structure has to change with a new value to obtain only one resonance frequency and a specific application. The main reason for using a varactor in WPT systems is to use one structure in multiple applications (medical, wireless sensors, and binary data), which is not achievable with the previous WPT system. With this idea, we can design a tunable WPT system for charging a mobile phone, wireless sensor, or biomedical device. In the simulation, the equivalent circuit of the varactor was used for realizing the varactor with the C_j as indicated in the data sheet of the SMV1405 (Hand and Cummer, 2010) to verify the capacity of the structure to tune the frequency model band. By changing the varactor capacitance from 2.67 to 0.63 pF, the studied TDB-WPT system will be tuned over a frequency range of 817 to 1018 MHz (Fig. 7).

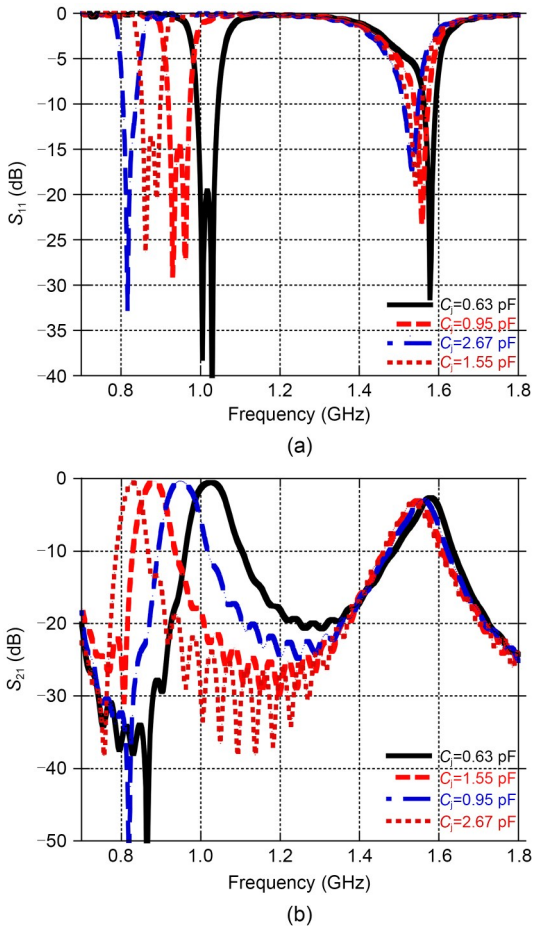

Fig. 7 Parameters of S_{11} (a) and S_{21} (b)

The system consists of two half symmetric rings. The performance of the system without a varactor is shown in Fig. 8a. The system has two symmetric resonance circuits that produce one band applicable to the higher frequency.

After adding the varactor on one side, the capacitance of the one-half ring circuit increases. According to the resonance equation $f_r=1/\left(2\pi\sqrt{LC}\right)$, the resonance frequency band of that circuit decreases and that band is then shifted to the lower frequency (Fig. 8b). Figs. 8b and 8c show how the two positions of the varactor will produce the same response due to the symmetry of the system. The length of the resonator can be calculated from $L=\pi r=20\pi$ mm, and the odd mode frequency from

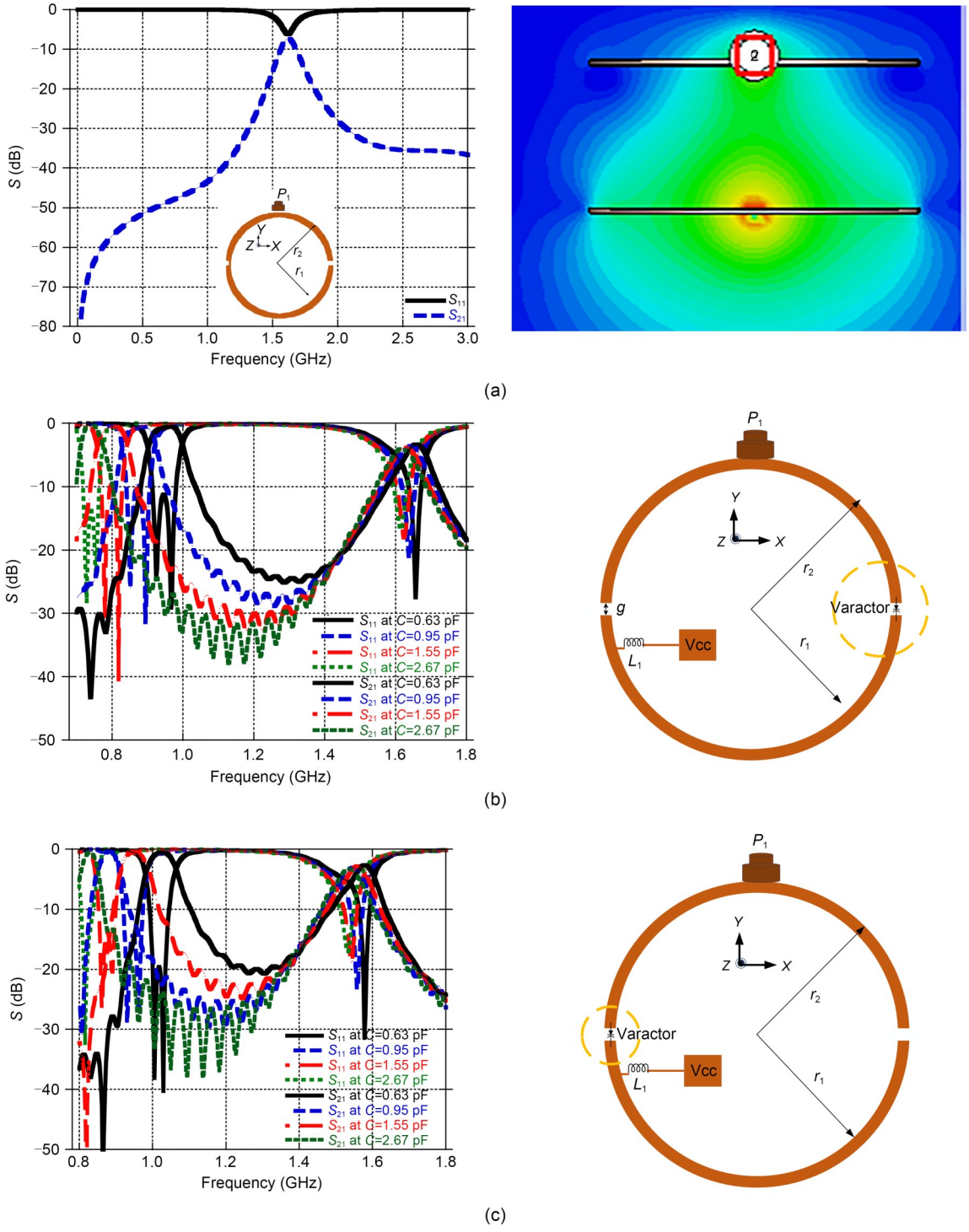

Fig. 8 Effect of the varactor position system without a varactor (a), system with a varactor in ring 1 (b), and system with a varactor in ring 2 (c)

$f_{\text{odd}}=c/\left(2L\sqrt{\varepsilon_{\text{eff}}}\right)=\dfrac{3\times10^{8}\ \text{m/s}}{40\pi\times10^{-3}\ \text{m}\times\sqrt{2.2}}=1.6$ GHz. For the odd mode excitation, there is a voltage null at the midpoint of the resonator, and the maximum field concentrates at the edges of the resonator. Therefore, the loading element is able to tune the frequency band at 1.6 GHz while the lower band is preserved (Atallah et al., 2016).

4 Transmission distance

The matching and coupling between Tx and Rx are changed when varying the transmission distance. To determine the optimum distance to transfer power, the simulation results at different transmission distances were compared. Fig. 9 highlights the S_{11} and S_{21} results for different transmission distances. At the short transmission distance of $h \leq 20$ mm, splitting occurs in the frequency response around the resonance frequency. At the long transmission distance of $h \geq 24$ mm, the coupling and matching between Tx and Rx are reduced, which decreases the coupling efficiency of the system.

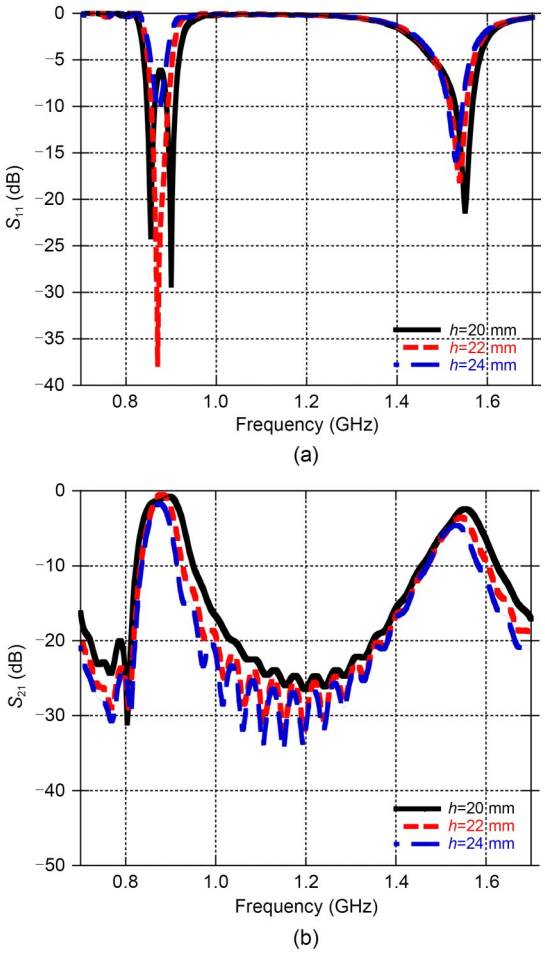

Fig. 9 S_{11} (a) and S_{21} (b) at transmission distances

The TDB-WPT system consists of two half rings that are responsible for producing the dual bands. One of the HR-DGSs which is loaded with a varactor (SMV1405) is responsible for the tuned band from 817 to 1018 MHz, while the other is responsible for the fixed band at 1.6 GHz. Fig. 10 illustrates the magnetic field distributions at the two operating bands.

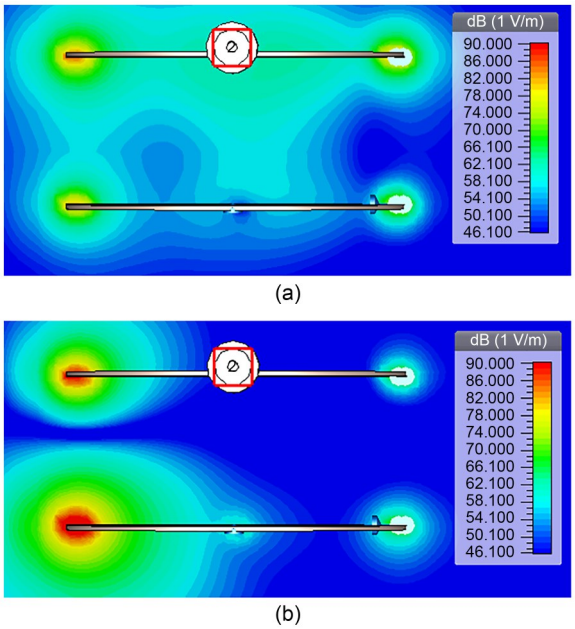

Fig. 10 Magnetic field distributions at 882 MHz (a) and the fixed band of 1.6 GHz (b)

The maximum attainable efficiency (η_{max}) is calculated using Eq. (3). It depends on the coupled Q-factor computed by Eq. (4) (Imura and Hori, 2011; Ohira, 2017), where R_{ES} is the equivalent scalar resistance and is computed using Eq. (5). The computed K_Q is 7.17 at 817 MHz and 2.70 at 1.6 GHz. Then, η_{max} equals 75% and 71%, separately.

$$\eta_{max}=\left[K_Q\Big/\left(1+\sqrt{1+K_Q^2}\right)\right]^2, \tag{3}$$

$$K_Q=|Z_{21}|/R_{ES}, \tag{4}$$

$$R_{ES}=\sqrt{R_{11}R_{22}-R_{21}R_{12}}, \tag{5}$$

where K_Q is the the coupled Q-factor of the coil as in Imura and Hori (2011) and Ohira (2017), and Z_{21} is the impedance in port 2 from port 1.

5 Misalignment

The effects of misalignment between the Tx and Rx resonators due to a horizontal shift in the X and Y

directions were studied (Fig. 11a) with the vertical distance fixed at h=22 mm. The best power transfer efficiency was attained at perfect alignment when there was no shift in the X and Y directions, as illustrated in Figs. 11b and 11c. For the Y shift, the coupling efficiency gradually degraded. However, a severe degradation in the coupling efficiency occurred at a shift of 6 mm for the X direction and in X=Y shift where the Rx resonator's greatest magnetic field intersected with the Tx resonator's minimum magnetic field. Details of the misalignment can be seen in Section 2 of the supplementary materials.

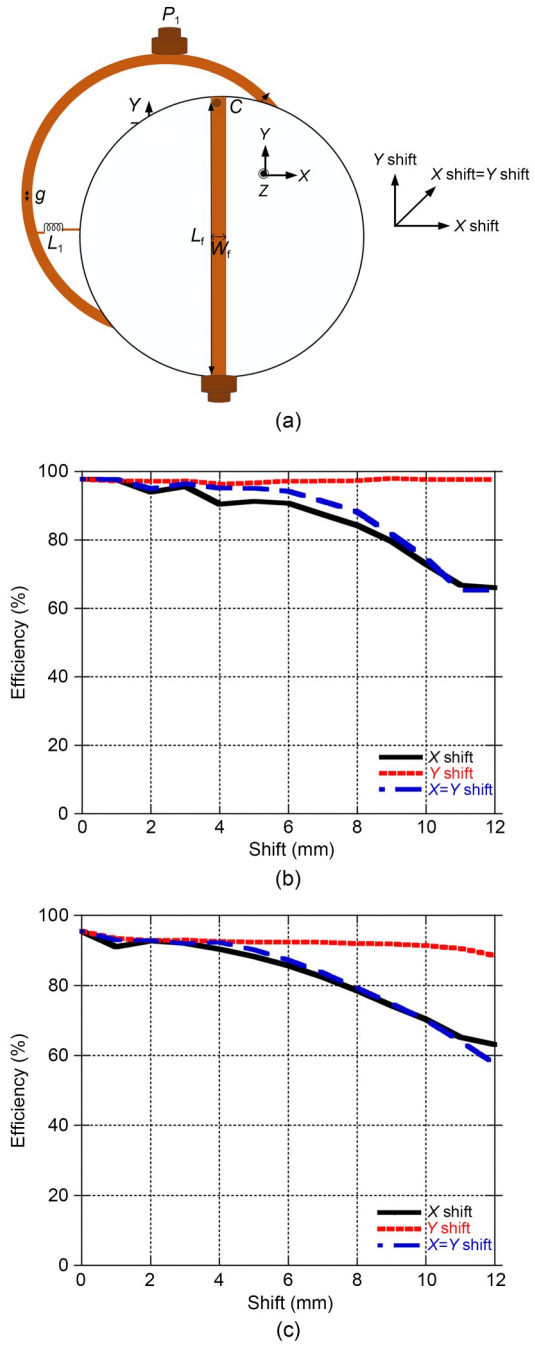

Fig. 11 Schematic of misalignment due to horizontal shift (a), electromagnetic (EM) simulated tunable dual band wireless power transfer (TDB-WPT) efficiency versus misalignment shifts in a tuned band (b), and EM simulated TDB-WPT efficiency versus misalignment shifts in a fixed band (c)

6 Experimental results

The studied system was manufactured and analyzed to achieve high wireless transmission with the frequency reconfiguration operation. Fig. 12a shows the top and bottom views of the fabricated prototype of the TDB-WPT system. The TDB-WPT system was fabricated on Rogers 5880 laminate with the previously indicated specifications. The measurement setup is illustrated in Fig. 12b. The two ports of the network analyzer were connected to the ports of the Tx and Rx circuits to measure the S-parameters. The S-parameters were used to describe the coupling between Tx and Rx and the matching in the system. Each part was connected to two green lines to bias the varactor. The positive of the DC power supply was connected to the cathode of the varactor in both the Tx and Rx to change the voltage at the same time, and then the resonance frequency was changed relative to the voltage, and the anode was connected to the green line to the 0 V (ground (GND)). The capacitance of the whole system changed when various voltage values were applied to the varactor diode, and hence the TDB-WPT system changed only the first resonance frequency without any change to the second resonance frequency. The varactor worked by connecting the cathode terminal to an inductor radio frequency (RF) choke, then a little bias wire, and finally a volt current condenser (Vcc) pad. The anode was connected to the GND (the same point of subminiature version A (SMA) connectors). The capacitance of the varactor was changed by changing the applied voltage. The bias line had a length of 15 mm and a width of 0.25 mm, which conferred sufficient high impedance, and was loaded by an RF choke inductor of 47 nH to isolate the DC and the RF signal. The measurement steps were applied using a network analyzer (N5222A) and the power supply. The measurement results are shown in Figs. 12c and 12d. Eqs. (6) and (7) were used to

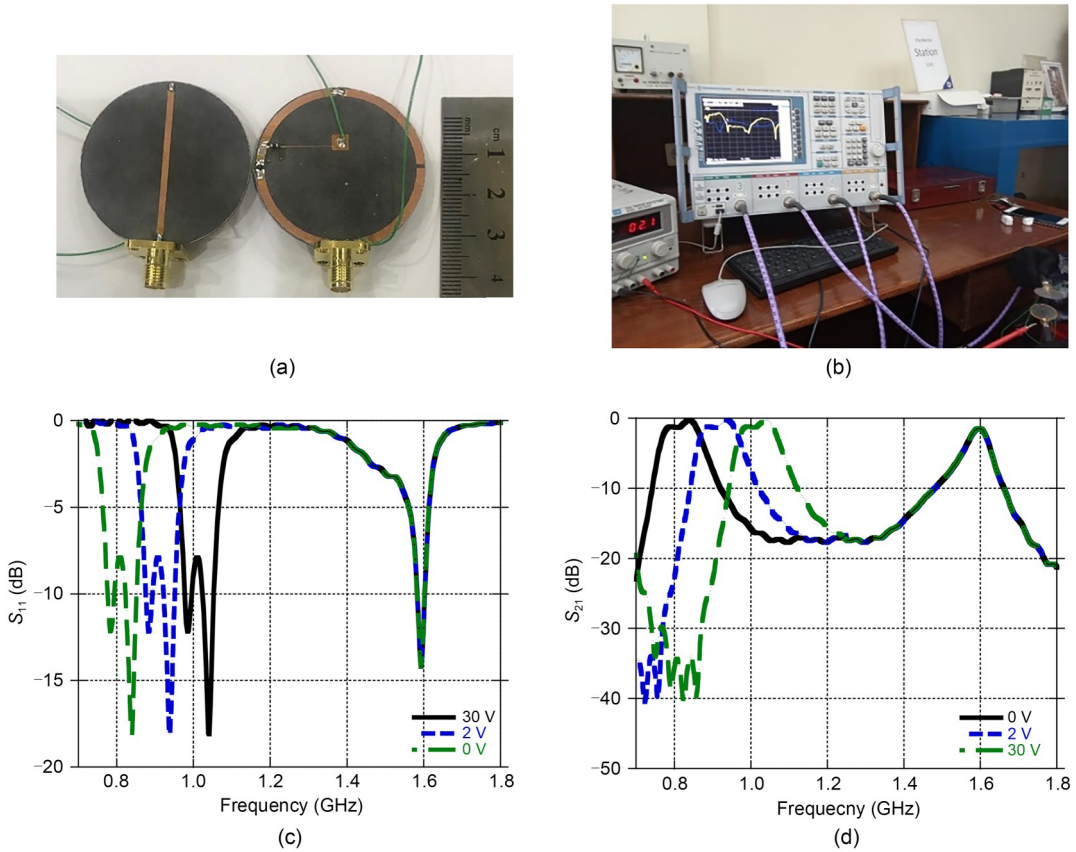

Fig. 12 Experiment measurements: (a) photograph of the tunable dual band wireless power transfer (TDB-WPT) system; (b) TDB-WPT system along with the setup; (c) measured S_{11}; (d) measured S_{21} (References to color refer to the online version of this figure)

compute the coupling efficiency and the FoM of the proposed system, respectively. FoM was used to compare the performance between multiple structures according to size (A), transmission distance (h), and coupling efficiency (η).

$$\eta=\frac{|s_{21}|^2}{1-|s_{11}|^2}, \tag{6}$$

$$\text{FoM}=\eta\frac{h}{\sqrt{A}}. \tag{7}$$

Fig. 12 shows that the system achieved coupling efficiencies of nearly 98% through the tuned band from 817 to 1018 MHz and 95% at the fixed band of 1.6 GHz. At the tuned band, the system achieved an average FoM of 0.53, while at the fixed band, it achieved an FoM of 0.52.

Fig. 13 compares the simulated and measured coupling efficiencies of the proposed design. The measured

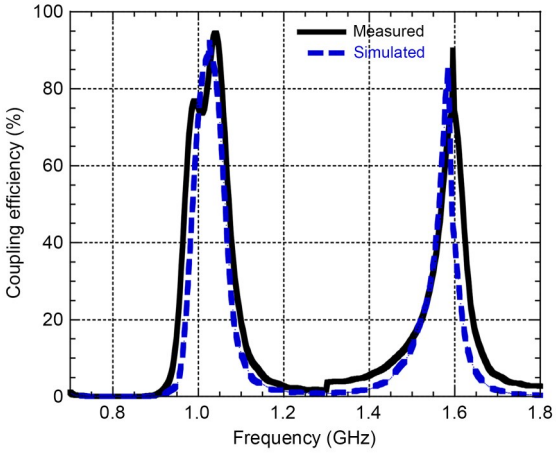

Fig. 13 Coupling efficiency versus frequency

S_{21} was around −0.1 dB at the tuned band, and the system achieved an efficiency of around 98% over this band, based on Eqs. (6) and (7). The observed S_{21} was −0.2 dB at the fixed band of 1.6 GHz with an efficiency of 95%. Table 2 compares the suggested system

Table 2 Comparison of the proposed wireless power transfer (WPT) system with other compact WPT systems

Reference	Frequency (MHz)	A (mm×mm)	h (mm)	η (%)	FoM	Tunability
Tahar et al., 2018	450	15×15	12.5	71	0.59	No
	950	15×15	12.5	73	0.60	No
Fereshtian and Ghalibafan, 2020	6.78	120×120	50	71	0.29	No
	13.56	120×120	50	56	0.23	No
Kung and Lin, 2020	13.50	100×100	20	71	0.14	No
	6.78	100×100	20	70	0.14	No
Kupreyev et al., 2019	ISM band	34×20	17.5	74	0.48	No
	ISM band	34×20	17.5	58	0.37	No
Atallah et al., 2020	280	20×20	6	91	0.27	No
	490	20×20	6	79	0.23	No
Sharaf et al., 2019	300	20×20	17	80	0.68	No
	675	20×20	17	73	0.62	No
Atallah et al., 2021	960	20×20	16	97	0.47	No
	1400	20×20	16	97	0.47	No
Tahar et al., 2017	300	30×15	16	71	0.76	No
	700	30×15	16	72	0.77	No
This study	817–1018	40×40	22	98	0.53	Yes
	1600	40×40	22	95	0.52	Yes

ISM: industrial scientific medical

with recently published WPT systems in terms of the frequency of operation, total area, transmission distance, coupling efficiency, FoM, and tunability function. Our proposed system performed well compared with other systems and achieved the tunability function, which is essential for recent multifunction WPT systems.

The matching at the lower frequency can be controlled using the varactor. Our proposed system achieved acceptable matching values over the tuned band range (Figs. 7b and 12d). The system can operate at any frequency within the tuned band with acceptable matching and coupling values. The system is suitable for operation in a single WPT application at one time, but it is not inconsistent with the operation of different applications at other times by changing the voltage applied to the cathode of the varactor. Details of multiple WPT applications can be seen in Section 3 of the supplementary materials.

The suggested structure is a printed circuit and is illustrated only as the coupling part between the Tx and Rx of the WPT system. The proposed design is considered as the coupling part of the whole WPT system, and the actual loads should be connected after adding the rectifier circuit. According to the resonance frequency, previous studies discussed the coupling part in specific applications (Kung and Lin, 2020; Atallah et al., 2021). We compared the coupling part of our system with those from recently published papers (Sharaf et al., 2019; Kung and Lin, 2020). In future work, the complete system will be studied and investigated from RF to DC rectifier.

7 Conclusions

In this study, a novel TDB-WPT system for short range application was presented, fabricated, and measured for validation purposes. The proposed TDB-WPT provided a wide tuning range of about 201 MHz from 817 to 1018 MHz at the first tuned band and a fixed band at 1.6 GHz. The dimensions were 40 mm×40 mm. Coupling efficiencies of 98% at the tuned band and 95% at the fixed band were obtained. Furthermore, the transmission distance was 22 mm, which is suitable for near-field applications.

Contributors

Hany A. ATALLAH designed the research. Rasha Hussein AHMED and Adel B. ABDEL-RAHMAN processed the data. Rasha Hussein AHMED drafted the paper. Hany A. ATALLAH and Rasha Hussein AHMED revised and finalized the paper.

Conflict of interest

All the authors declare that they have no conflict of interest.

Data availability

The data that support the findings of this study are available from the corresponding author upon reasonable request.

References

Abdel-Rahman A, Verma AK, Boutejdar A, et al., 2004. Compact stub type microstrip bandpass filter using defected ground plane. *IEEE Microw Wirel Compon Lett*, 14(4):136-138. https://doi.org/10.1109/LMWC.2003.821503

Ahn D, Ghovanloo M, 2016. Optimal design of wireless power transmission links for millimeter-sized biomedical implants. *IEEE Trans Biomed Circ Syst*, 10(1):125-137. https://doi.org/10.1109/TBCAS.2014.2370794

Atallah HA, Abdel-Rahman AB, Yoshitomi K, et al., 2016. Compact frequency reconfigurable filtennas using varactor loaded T-shaped and H-shaped resonators for cognitive radio applications. *IET Microw Antenn Propag*, 10(9):991-1001. https://doi.org/10.1049/iet-map.2015.0700

Atallah HA, Huseein R, Abdel-Rahman AB, 2019. Novel and compact design of capacitively loaded C-shaped DGS resonators for dual band wireless power transfer (DB-WPT) systems. *AEU-Int J Electron Commun*, 100:95-105. https://doi.org/10.1016/j.aeue.2018.12.016

Atallah HA, Hussein R, Abdel-Rahman AB, 2020. Compact coupled resonators for small size dual-frequency wireless power transfer (DF-WPT) systems. *IET Microw Antenn Propag*, 14(7):617-628. https://doi.org/10.1049/iet-map.2018.5693

Atallah HA, El Negm Yousef MMA, Abdel-Rahman AB, 2021. Efficiency improvement of dual-band wireless power transfer (DB-WPT) system with U-shape resonator and capacitively loaded E-shape defected ground structure (DGS). *Wirel Pers Commun*, 119(3):2083-2091. https://doi.org/10.1007/S11277-021-08319-0

Barakat A, Yoshitomi K, Pokharel RK, 2019. Design and implementation of dual-mode inductors for dual-band wireless power transfer systems. *IEEE Trans Circ Syst II Expr Briefs*, 66(8):1287-1291. https://doi.org/10.1109/TCSII.2018.2883671

Belo D, Correia R, Pereira F, et al., 2017. Dual band wireless power and data transfer for space-based sensors. Topical Workshop on Internet of Space, p.1-4. https://doi.org/10.1109/TWIOS.2017.7869773

Dautov K, Hashmi M, Nauryzbayev G, et al., 2020. Recent advancements in defected ground structure-based near-field wireless power transfer systems. *IEEE Access*, 8:81298-81309. https://doi.org/10.1109/ACCESS.2020.2991269

Dautov K, Hashmi M, Nauryzbayev G, et al., 2021. Compact multi-frequency system design for SWIPT applications. *Int J RF Microw Comput Aid Eng*, 31(6):e22632. https://doi.org/10.1002/MMCE.22632

del Prete M, Berra F, Costanzo A, et al., 2015. Exploitation of a dual-band cell phone antenna for near-field WPT. IEEE Wireless Power Transfer Conf, p.1-4. https://doi.org/10.1109/WPT.2015.7139132

Fereshtian A, Ghalibafan J, 2020. Impedance matching and efficiency improvement of a dual-band wireless power transfer system using variable inductance and coupling method. *AEU-Int J Electron Commun*, 116:153085. https://doi.org/10.1016/j.aeue.2020.153085

Garnica J, Chinga RA, Lin J, 2013. Wireless power transmission: from far field to near field. *Proc IEEE*, 101(6):1321-1331. https://doi.org/10.1109/JPROC.2013.2251411

Hand TH, Cummer SA, 2010. Reconfigurable reflectarray using addressable metamaterials. *IEEE Antenn Wirel Propag Lett*, 9:70-74. https://doi.org/10.1109/LAWP.2010.2043211

Hekal S, Abdel-Rahman AB, Jia HT, et al., 2017. A novel technique for compact size wireless power transfer applications using defected ground structures. *IEEE Trans Microw Theory Tech*, 65(2):591-599. https://doi.org/10.1109/TMTT.2016.2618919

Hu H, Georgakopoulos SV, 2015. Wireless power transfer in human tissue via conformal strongly coupled magnetic resonance. IEEE Wireless Power Transfer Conf, p.1-4. https://doi.org/10.1109/WPT.2015.7140150

Huang SY, Lee YH, 2009. A compact E-shaped patterned ground structure and its applications to tunable bandstop resonator. *IEEE Trans Microw Theory Tech*, 57(3):657-666. https://doi.org/10.1109/TMTT.2009.2013313

Huh J, Lee SW, Lee WY, et al., 2011. Narrow-width inductive power transfer system for online electrical vehicles. *IEEE Trans Power Electron*, 26(12):3666-3679. https://doi.org/10.1109/TPEL.2011.2160972

Imura T, Hori Y, 2011. Maximizing air gap and efficiency of magnetic resonant coupling for wireless power transfer using equivalent circuit and Neumann formula. *IEEE Trans Ind Electron*, 58(10):4746-4752. https://doi.org/10.1109/TIE.2011.2112317

Jeshma TV, George B, 2020. MR sensor-based coil alignment sensing system for wirelessly charged EVs. *IEEE Sens J*, 20(10):5588-5596. https://doi.org/10.1109/JSEN.2020.2969432

Jolani F, Yu YQ, Chen ZZ, 2014. A planar magnetically coupled resonant wireless power transfer system using printed spiral coils. *IEEE Antenn Wirel Propag Lett*, 13:1648-1651. https://doi.org/10.1109/LAWP.2014.2349481

Kung ML, Lin KH, 2020. A dual-band wireless power transfer system with efficiency-boosting converter. *IEEE Microw Wirel Compon Lett*, 30(11):1108-1111. https://doi.org/10.1109/LMWC.2020.3027553

Kung ML, Chen FY, Lin KH, 2019. Near-field wireless power transfer system with efficiency tracking for dual-band applications. IEEE 8th Global Conf on Consumer Electronics, p.610-611. https://doi.org/10.1109/GCCE46687.2019.9015611

Kupreyev D, Dautov K, Hashmi M, et al., 2019. Design of a compact DGS based dual-band RF WPT system for low-power applications. 8th Asia-Pacific Conf on Antennas and Propagation, p.48-49. https://doi.org/10.1109/APCAP47827.2019.9471919

Lee WS, Park S, Lee JH, et al., 2019. Longitudinally misalignment-insensitive dual-band wireless power and data transfer

systems for a position detection of fast-moving vehicles. *IEEE Trans Antenn Propag*, 67(8):5614-5622. https://doi.org/10.1109/TAP.2019.2916697

Liu M, Chen MJ, 2019. Dual-band multi-receiver wireless power transfer: architecture, topology, and control. IEEE Applied Power Electronics Conf and Exposition, p.851-859. https://doi.org/10.1109/APEC.2019.8721837

Liu Y, Jäntti R, 2006. A study towards enhanced reliability performance of remote control and monitoring application over commercial wireless communication networks. Int Conf on Wireless Communications, Networking and Mobile Computing, p.1-4. https://doi.org/10.1109/WiCOM.2006.385

Minnaert B, Stevens N, 2018. Maximizing the power transfer for a mixed inductive and capacitive wireless power transfer system. IEEE Wireless Power Transfer Conf, p.1-4. https://doi.org/10.1109/WPT.2018.8639265.

Ohira T, 2017. The kQ product as viewed by an analog circuit engineer. *IEEE Circ Syst Mag*, 17(1):27-32. https://doi.org/10.1109/mcas.2016.2642698

Saad MR, Tahar F, Chalise S, et al., 2018. High FoM dual band wireless power transfer using bow-tie defected ground structure resonators. IEEE Wireless Power Transfer Conf, p.1-4. https://doi.org/10.1109/WPT.2018.8639134

Sharaf R, Abdel-Rahman AB, Abd El-Hameed AS, et al., 2019. A new compact dual-band wireless power transfer system using interlaced resonators. *IEEE Microw Wirel Compon Lett*, 29(7):498-500. https://doi.org/10.1109/LMWC.2019.2917747

Sun WX, Liu CL, Zhu JY, 2018. A remote controlled mobile robot based on wireless transmission. 2nd IEEE Advanced Information Management, Communicates, Electronic and Automation Control Conf, p.2173-2176. https://doi.org/10.1109/IMCEC.2018.8469731

Tahar F, Barakat A, Saad R, et al., 2017. Dual-band defected ground structures wireless power transfer system with independent external and inter resonator coupling. *IEEE Trans Circ Syst II Expr Briefs*, 64(12):1372-1376. https://doi.org/10.1109/TCSII.2017.2740401

Tahar F, Chalise S, Yoshitomi K, et al., 2018. Compact dual-band wireless power transfer using overlapped single loop defected ground structure. IEEE Wireless Power Transfer Conf, p.1-4. https://doi.org/10.1109/WPT.2018.8639281

Verma S, Rano D, Malhotra S, et al., 2021. Measurements and characterization of a newly developed novel miniature WIPT system. *IEEE Trans Instrum Meas*, 70:2004211. https://doi.org/10.1109/TIM.2021.3075537

Wang GX, Liu WT, Sivaprakasam M, et al., 2005. Design and analysis of an adaptive transcutaneous power telemetry for biomedical implants. *IEEE Trans Circ Syst I Regul Pap*, 52(10):2109-2117. https://doi.org/10.1109/TCSI.2005.852923

Xu SH, Zhang H, Yao C, et al., 2019. Eigenvector lookup position detection method for wireless power transfer of electric vehicles. IEEE PELS Workshop on Emerging Technologies: Wireless Power Transfer, p.177-180. https://doi.org/10.1109/WoW45936.2019.9030642

Yang CL, Chang CK, Lee SY, et al., 2017. Efficient four-coil wireless power transfer for deep brain stimulation. *IEEE Trans Microw Theory Tech*, 65(7):2496-2507. https://doi.org/10.1109/TMTT.2017.2658560

List of supplementary materials

1 DB J-inverter ECM
2 Angular misalignment
3 Multiple WPT applications